REPRESENTATION OF ION COMPOSITION IN IRI

Vladimir Truhlik

Department of the Ionosphere and Aeronomy
Institute of Atmospheric Physics, Academy of Sciences of the Czech Republic
Praha, Czech Republic
Email : vtr@ufa.cas.cz

Outline

- Basic theoretical description
- Measurement of ion composition
- Representation of ion composition in IRI
  - The upper transition height
- Summary

Ion composition

Photoionization

$$X + h\nu \rightarrow X^+ + e$$

O,N,O_2,N_2,He

O^+,N^+,O_2^+,N_2^+,He^+,…

Table 1: Photoionisation processes

No.	Reaction	Rate*
1	$O + h\nu \longrightarrow O^+(^4S) + e$	q_1
2	$O + h\nu \longrightarrow O^+(^2D) + e$	q_2
3	$O + h\nu \longrightarrow O^+(^2P) + e$	q_3
4	$O + h\nu \longrightarrow O^+(^4P) + e$	q_4
5	$O + h\nu \longrightarrow O^+(^2P^*) + e$	q_5
6	$N + h\nu \longrightarrow N^+ + e$	q_6
7	$O_2 + h\nu \longrightarrow O_2^+ + e$	q_7
8	$N_2 + h\nu \longrightarrow N_2^+ + e$	q_8
9	$N_2 + h\nu \longrightarrow N^+ + N + e$	q_9
10	$He + h\nu \longrightarrow He^+ + e$	q_{10}
11	$O + h\nu \longrightarrow O^{++} + 2e$	q_{11}
12	$O^+ + h\nu \longrightarrow O^{++} + e$	q_{12}

Ion composition – ion molecule reactions

Table 2: Ion-molecule reactions

No.	Reaction	Rate constant [$cm^3 s^{-1}$]
1	$O^+(^4S) + N_2 \rightarrow NO^+ + N$	$k_{1a} = 1{,}533.10^{-12} - 5{,}92.10^{-13}\left(\frac{T_{eff}}{300}\right) + 8{,}60.10^{-14}\left(\frac{T_{eff}}{300}\right)^2$ $300K \le T_{eff} \le 1700K$
		$k_{1b} = 2{,}73.10^{-12} - 1{,}155.10^{-12}\left(\frac{T_{eff}}{300}\right) + 1{,}483.10^{-13}\left(\frac{T_{eff}}{300}\right)^2$ $1700K < T_{eff} < 6000K$
2	$O^+(^4S) + O_2 \rightarrow O_2^+ + O$	$k_2 = 1{,}7.10^{-11}\left(\frac{300}{T_{eff}}\right)^{0{,}77} + 8{,}54.10^{-11}\, e^{\left(-\frac{3467}{T_{eff}}\right)}$ $300K \le T_{eff} \le 1800K$
3	$O^+(^4S) + e \rightarrow O + h\nu$	$k_3 = 4{,}0.10^{-12}\left(\frac{T_e}{300}\right)^{-0{,}7}$
4	$O^+(^4S) + H \rightarrow H^+ + O$	$k_4 = 2{,}2.10^{-11} T_e^{0{,}5}$
5	$O^+(^2D) + N_2 \rightarrow N_2^+ + O$	$k_5 = 8.10^{-10}$
6	$O^+(^2D) + O_2 \rightarrow O_2^+ + O$	$k_6 = 7.10^{-10}$
7	$O^+(^2D) + O \rightarrow O^+(^4S) + O$	$k_7 = 5.10^{-12}$
8	$O^+(^2D) + e \rightarrow O^+(^4S) + e$	$k_8 = 6{,}6.10^{-8}\left(\frac{300}{T_e}\right)^{0{,}5}$
9	$O^+(^2P) + O \rightarrow O^+(^4S) + O$	$k_9 = 4.10^{-10}$
10	$O^+(^2P) + N_2 \rightarrow N_2^+ + O$	$k_{10} = 3{,}4.10^{-10}$
11	$O^+(^2P) + e \rightarrow O^+(^2D) + e$	$k_{11} = 1{,}5.10^{-7}\left(\frac{300}{T_e}\right)^{0{,}5}$
12	$O^+(^2P) + e \rightarrow O^+(^4S) + e$	$k_{12} = 4{,}7.10^{-8}\left(\frac{300}{T_e}\right)^{0{,}5}$
13	$O^+(^2P) \rightarrow O^+(^2D) + h\nu$	$k_{13} = 0{,}173\, s^{-1}$
14	$O^+(^2P) \rightarrow O^+(^4S) + h\nu$	$k_{14} = 0{,}047\, s^{-1}$
15	$N_2^+ + O \rightarrow O^+(^4S) + N_2$	$k_{15} = 9{,}8.10^{-12}\left(\frac{300}{T_i}\right)^{0{,}23}$
16	$N_2^+ + O \rightarrow NO^+ + N$	$k_{16} = 1{,}4.10^{-10}\left(\frac{300}{T_i}\right)^{0{,}44}$
17	$N_2^+ + O_2 \rightarrow O_2^+ + N_2$	$k_{17} = 9{,}1.10^{-11}\exp(-0.002\, T_{eff})$
18	$N_2^+ + e \rightarrow N + N$	$k_{18} = 2{,}7.10^{-7}$
19	$O_2^+ + NO \rightarrow NO^+ + O_2$	$k_{19} = 4{,}4.10^{-10}$
20	$O_2^+ + N \rightarrow NO^+ + O$	$k_{20} = 1{,}2.10^{-10}$
21	$O_2^+ + e \rightarrow O + O$	$k_{21a} = 2.10^{-7}\left(\frac{300}{T_e}\right)^{0{,}7}$ $T_e < 1200K$
		$k_{21b} = 1{,}6.10^{-7}\left(\frac{300}{T_e}\right)^{0{,}55}$ $T_e \ge 1200K$
22	$NO^+ + e \rightarrow N + O$	$k_{22} = 4{,}3.10^{-7}\left(\frac{300}{T_e}\right)$
23	$N^+ + O_2 \rightarrow NO^+ + O$	$k_{23} = 2.10^{-10}$
24	$N^+ + O_2 \rightarrow O_2^+ + N$	$k_{24} = 4.10^{-10}$
25	$N^+ + O_2 \rightarrow O^+(^4S) + NO$	$k_{25} = 3.10^{-11}$
26	$N^+ + O \rightarrow O^+(^4S) + N$	$k_{26} = 1.10^{-12}$
27	$H^+ + O \rightarrow O^+(^4S) + H$	$k_{27} = 2{,}5.10^{-11} T_e^{0{,}5}$
		He^+
28	$He^+ + N_2 \rightarrow N^+ + N + He$	$k_{28} = 1{,}0.10^{-9}$
29	$He^+ + N_2 \rightarrow N_2^+ + He$	$k_{29} = 6{,}5.10^{-10}$
30	$He^+ + O_2 \rightarrow O^+ + O + He$	$k_{30} = 1{,}1.10^{-9}$
		O^{++}
31	$O^{++} + N_2 \rightarrow O^+ + products$	$k_{31} = 1{,}3.10^{-9}$
32	$O^{++} + O \rightarrow O^+ + O^+$	$k_{32} = 6{,}6.10^{-11}$

F_2 region

$$Ne \approx [O^+] \propto \frac{[O]}{[N_2]}$$

O^+

N_2^+

O_2^+

NO^+

N^+

He^+

O^{++}

$$H^+ + O \underset{k2}{\overset{k1}{\rightleftharpoons}} O^+ + H$$

Plasmasphere formation

Ion composition

- Above ~200 km plasma tends to move along magnetic filed lines
  - Continuity equation (for the *s*th ion)

$$\frac{\partial n_s}{\partial t} + \frac{1}{A}\frac{\partial A n_s u_s'}{\partial s} = P_s - L_s,$$

n-density
A-cross section of the flux tube
u-velocity of particles
P, L - Production and loss

  - Momentum equation

$$n_s u_s' = -D_s \frac{\partial n_s}{\partial s} + F_s n_s,$$

n-density
u-velocity of particles
D-diffusion coefficient
F-external forces (gravity, drag etc.

To solve these equations - plasma temperatures are needed (plus neutral compositio
winds and drifts)

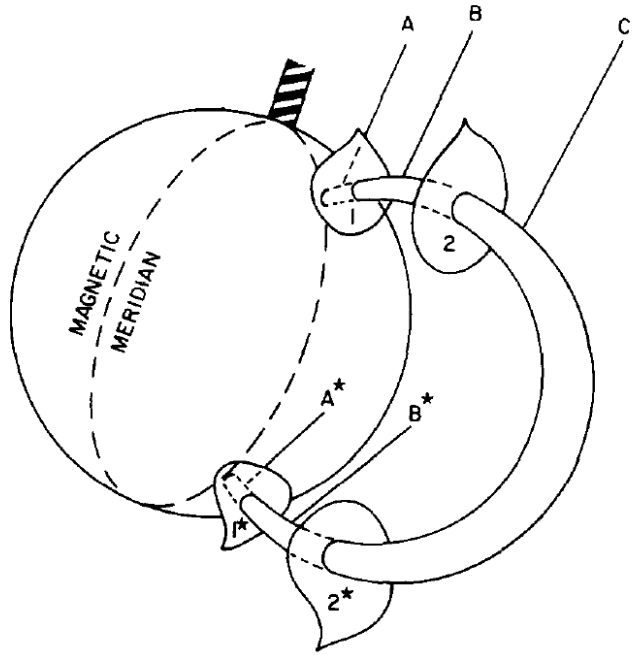

- Two possible simplifications:
  - Lower ionosphere (under F2) - photochemical equilibrium only => only ion molecule reactions (+EUV spectrum etc., neutral composition and temperature – MSIS) (region A)
  - In topside and plasmasphere if production, transport and loss neglected => diffusive equilibrium (height profiles determined by plasma scale height) (region C)

Measurement of ion composition

- Incoherent Scatter Radar (data mostly from Arecibo only)
- Retarding potential analyser or planar sensor (RPA, IVM) (in-situ measurements)
- i-th ion flux

$$\phi_i(P) = \frac{N_i}{2} V_r \left[1 + erf(\beta_i f_i) + \frac{1}{\sqrt{\pi}\beta_i V_r} \exp\left(-\beta_i^2 f_i^2\right) \right]$$

$$\beta_i = \left(m_i / 2kT_i \right)^{1/2} \qquad f_i = V_r - \left(2P / m_i \right)^{1/2}$$

Only major ions (in topside O^+, H^+, sometimes also He^+ (high solar activity; lower ionosphere also molecular ions)

RPA cannot distinguish between O^+ and N^+ etc.

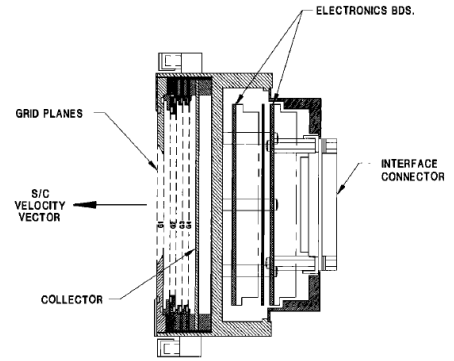

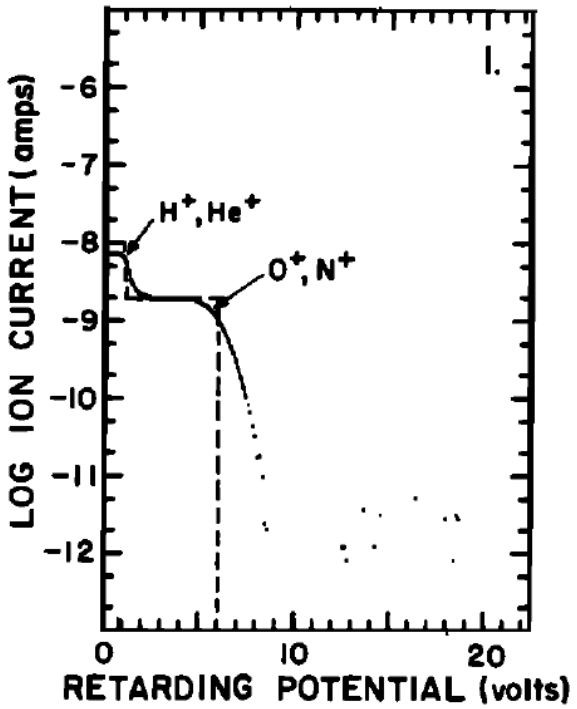

Measurement of ion composition II

- Ion mass spectrometer (IMS)
- Bennett, magnetic…
  - Complicated and heavy instruments
- IMS can distinguish among many ions – ion spectra
- Relative measurement => calibrate Ni (sum of individual ions) to Ne (e.g., from Langmuir probe)

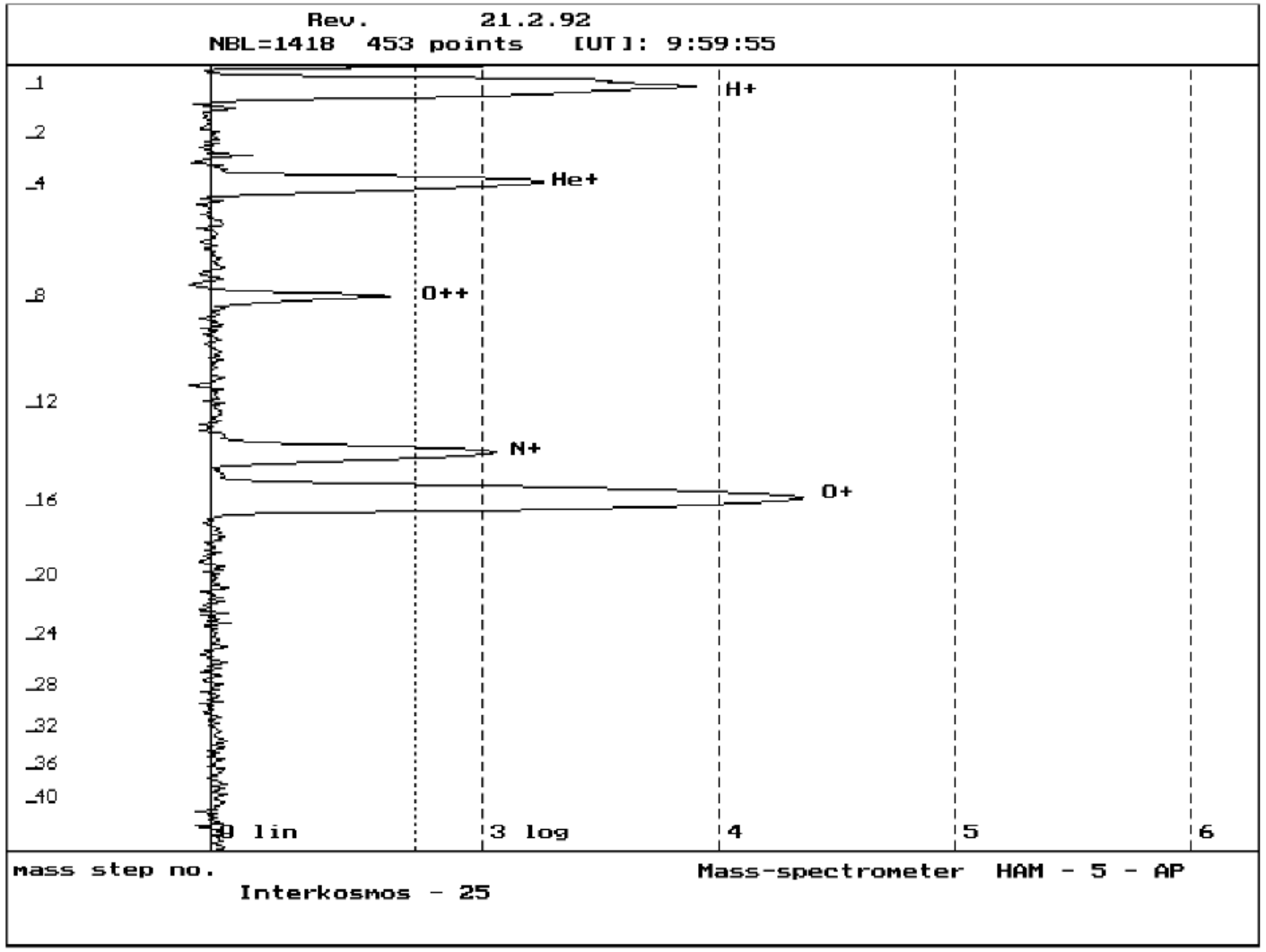

IRI - ion composition

- IRI includes representation of ion somposition
- IRI (2020 the latest version)
- Topside (above F_2 up to ~2000km - relative density of O^+, H^+, He^+, N^+ in dependence on geophysical parameters) :
  - TBT-15 (Truhlik, Bilitza, Triskova, ASR 2015)
  - DY-1985 (Danilov and Yaichnikov, 1985)
- Bottomside (up to F_2, relative density O^+, NO^+, O_2^+, N^+)
  - RBV-2010 (Richards, Bilitza, and Voglozin, RS, 2010)
  - DS-1995 (Danilov and Smirnova, ASR, 1995)
- IRI option – FORTRAN code - JF switch - JF(6)
  - .true. DS-1995 & DY-1985
  - .false. RBV-2010 & TBT-15(default option)

IRI topside ion composition model

TBT-15 (Truhlik, Bilitza, Triskova, ASR 2015, included in IRI from v.2016)

Empirical model of O^+, H^+, He^+, N^+ relative densities

Evolved from TTS-03 (Triskova, Truhlik, Smilauer,

(ASR Vol.31, No.3, 653, 2003)

Data used:

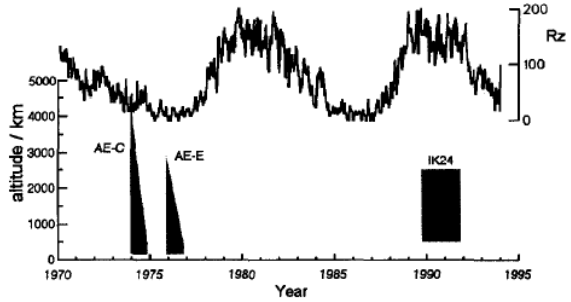

Periods of available data from the AE-C, AE-E and IK 24 satellites with corresponding solar activity, and altitude ranges.

solar activity	average F10.7	satellite	altitude km	inclination deg	time period	ion mass spectrometer
maximum	200	IK-24	500 - 2500	83	Nov 1989 - May 1991	Bennett
minimum	85	AE-C	350 - 1150	68	Dec 1973 - Nov 1974	Bennett + magnetic
minimum	75	AE-E	350 - 1150	20	Dec 1975 - Oct 1976	Bennett + magnetic

TBT-15 also includes results from C/NOFS at low latitudes

The full model consists of sub-models for individual altitude ranges and seasons

HSA: 550 ± 80 km, 900 ± 100 km, 1500 ± 150 km, and 2250 ± 250 km

LSA: 400 ± 50 km, 550 ± 70 km, 750 ± 90 km, and 1000 ± 150 km

Ion composition maps (LT vs latitude)

All available data for corresponding seasons (about 9 week periods centered on equinoxes and solstices) were selected. Data from summer and winter hemispheres were coupled for solstices, for equinoxes data from both hemispheres were put together and symmetry was assumed. A system of associated Legendre polynomials up to the 6th order is employed as a modeling function:

$$\log_{10}\frac{N_i}{N_T} = \sum_{l=0}^{6}\left\{a_l^0 P_l^0(\cos\theta) + \sum_{m=1}^{l}\left[a_l^m \cos m\varphi + b_l^m \sin m\varphi\right] P_l^m(\cos\theta)\right\},$$

P_l^m = associated Legendre function
θ = invdip colatitude (0..π), φ = magnetic local time (0..2π)
N_i = O^+, H^+, He^+ or N^+ density, N_T = total ion density ($\sum N_i$).

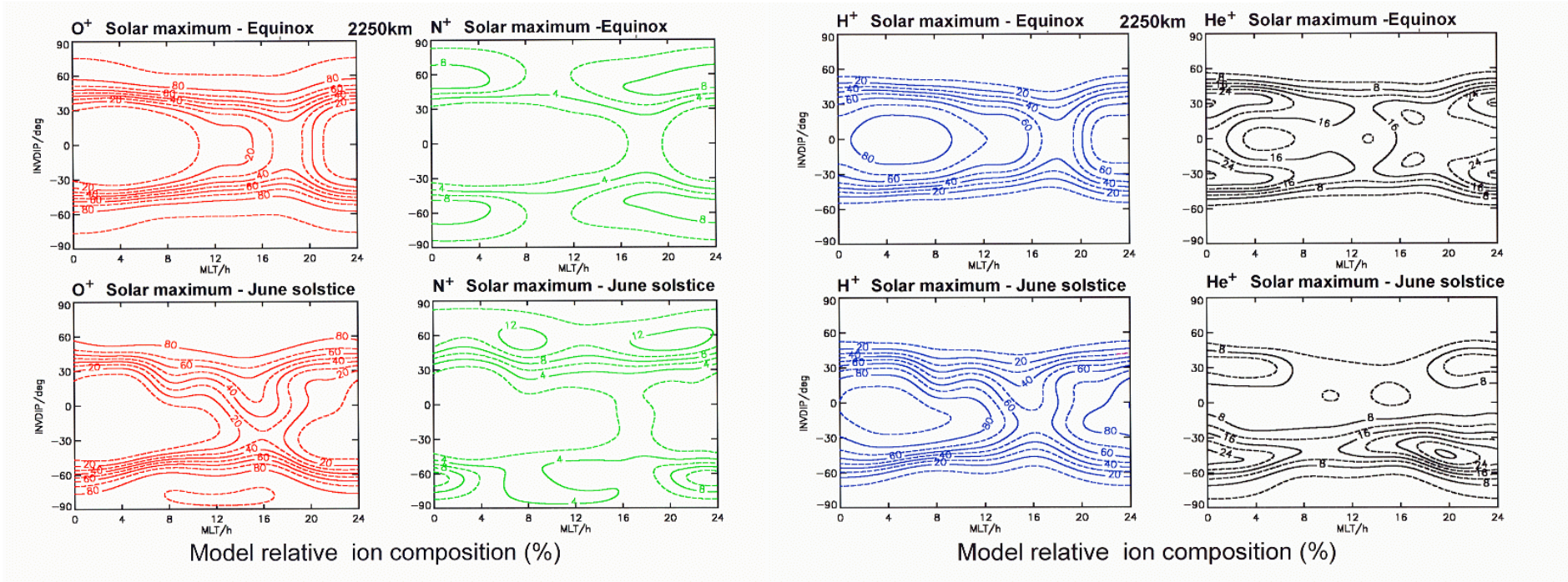

Example of contour plots

Vertical profiles

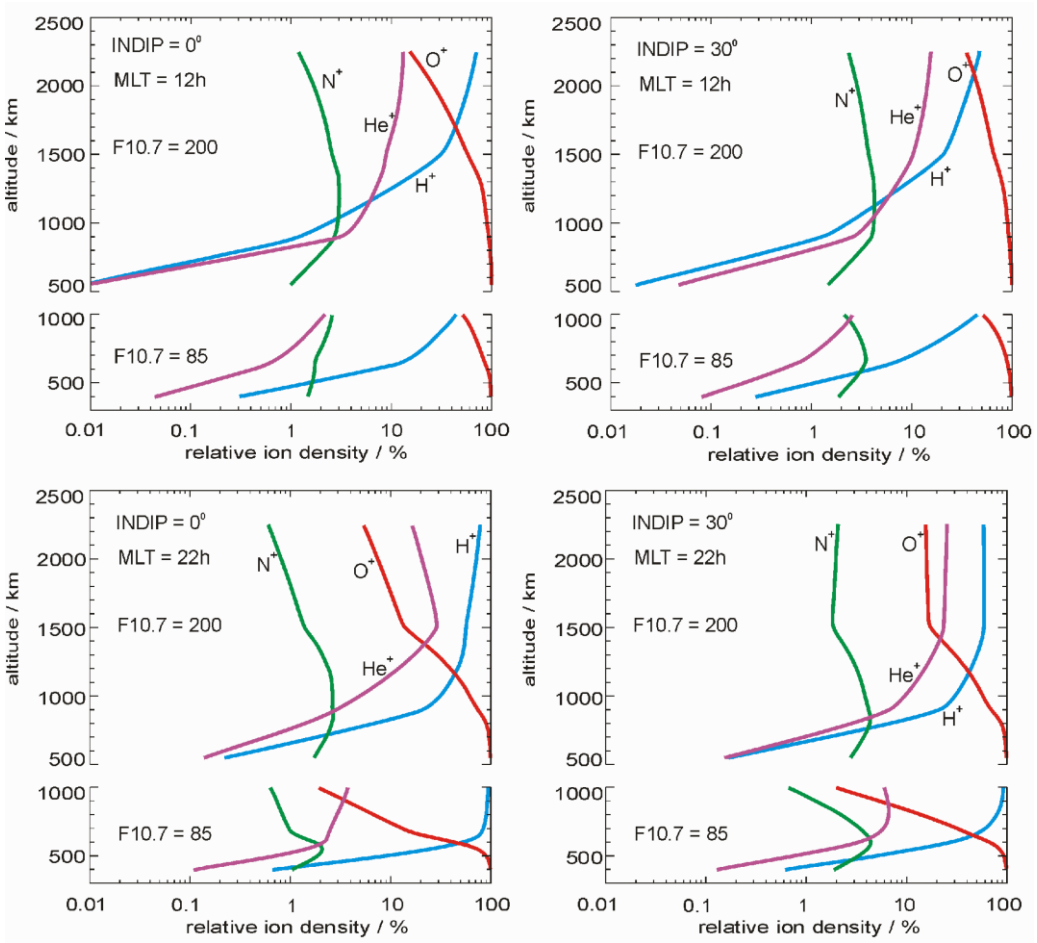

Examples of equinoctial vertical profiles of the relative ion densities calculated from the TTS model for high (F10.7=200) and low solar activity (F10.7=85) and for two local times (12 h and 22 h) and two latitudes (0 and 30deg).

Solar activity dependence

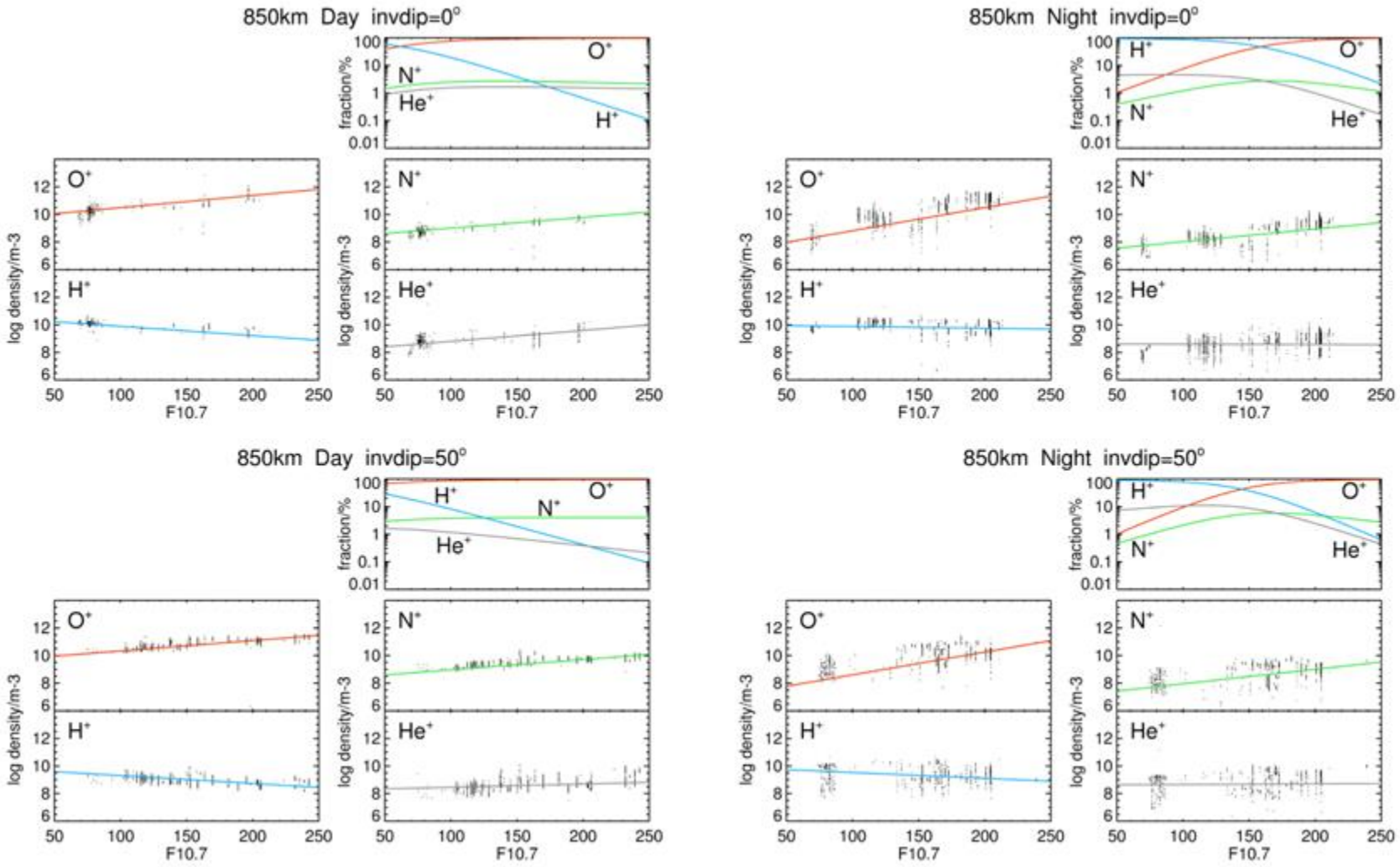

Absolute densities of individual ions on log scale are close to linear dependence on solar activity (F10.7 index).
Dependence of the logarithm of the individual ion densities from Atmosphere Explorer C&E and Intercosmos 24, and of the relative ion densities on the solar activity level characterized by the actual day values of the F10.7 index. Example for equinox, equator±15deg, mid-latitudes 50±15deg, altitude of 850±90 km, daytime and nighttime. Points-measured values, lines-values fitting. (Truhlik et al., Ann. Geophys, 2005)

He^+ vs. H^+ and He^+ dominance

He^+ is usually a minor ion in the topside ionosphere and plasmasphere
-low solar activity $[He^+]/[H^+] \approx 0.1$
but
-high solar activity $[He^+]/[H^+]$ in the topside ionosphere can be >1 and even at the same time $[He^+]/[O^+] > 1$ => He^+ is dominant
-middle-latitudes at nighttime

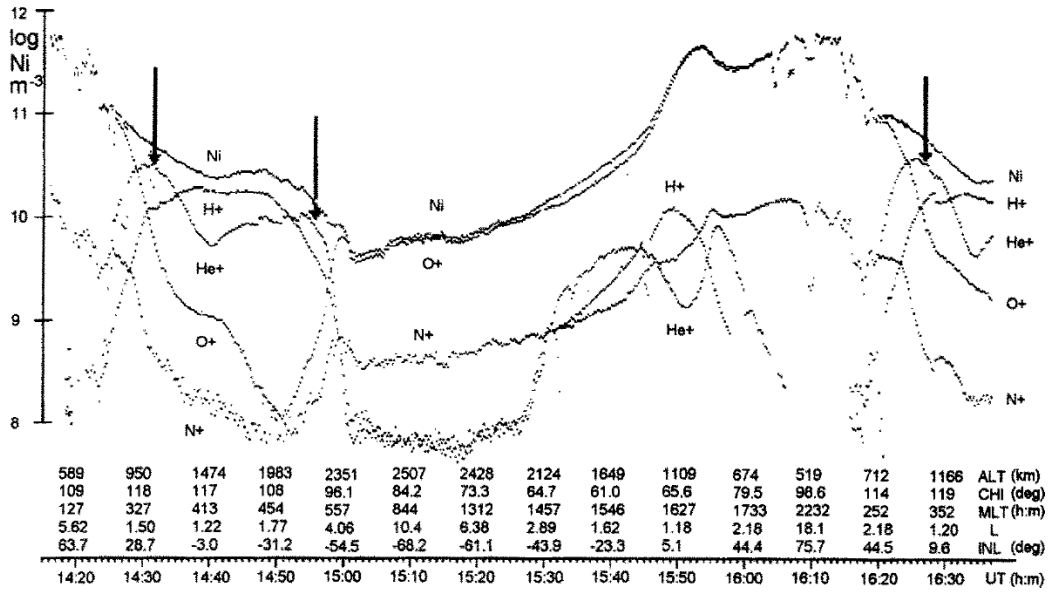

Example of ion composition with three major ions (O^+, H^+, and He^+) measured by ion mass spectrometer onboard the Intercosmos 24 satellite. Dominance of He^+ marked by arrows. (ALT - altitude, CHI - solar zenith angle, MLT - magnetic local time, L - McIlwain parameter, INL - invariant latitude, UT - Universal Time - 14.3.1991).

IRI TTS-03

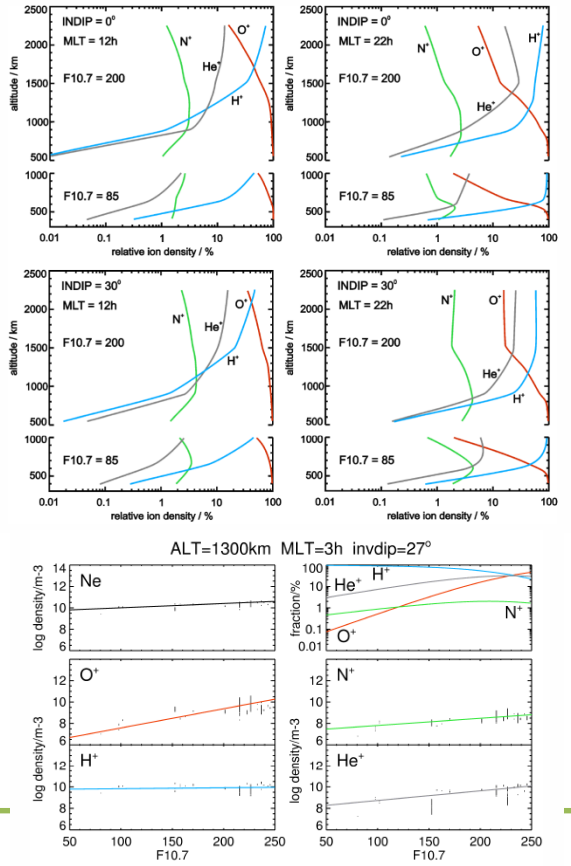

IRI bottomside RBV-2010

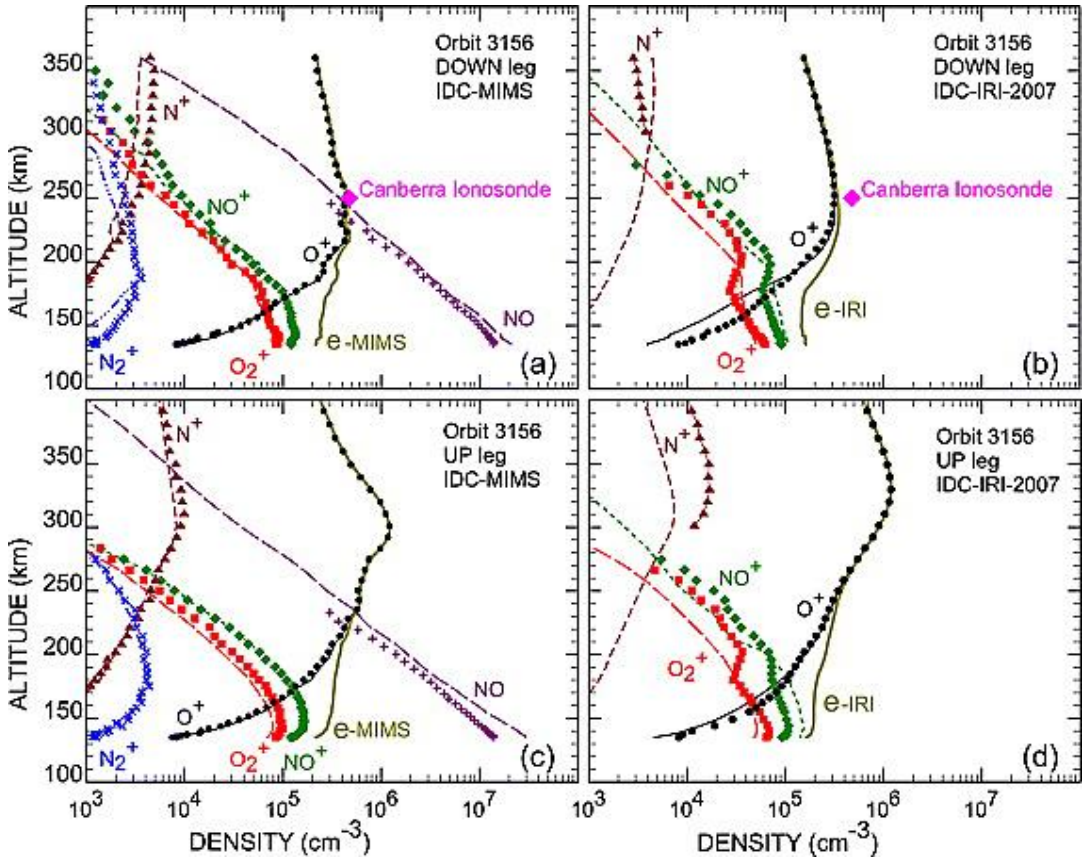

Richards, Bilitza, and Voglozin, RS, 2010

Comparison of ion and electron densities for the down leg and up leg portions of AE-C Orbit 3156 on 12 September 1974. (a) The IDC (=RBV-2010) model (lines) and AE-C MIMS data (symbols) for the down leg with the IDC model using the MIMS measured electron densities and the OSS measured neutral densities. (b) The IDC and IRI model densities for the down leg with IDC using the IRI electron densities and the NRLMSISE-00 model neutral densities. (c and d) The same comparisons as Figures 2a and 2b for the up leg. The large diamond shows the N_mF_2 measured by the Canberra ionosonde.

IRI-2020 topside+bottomside

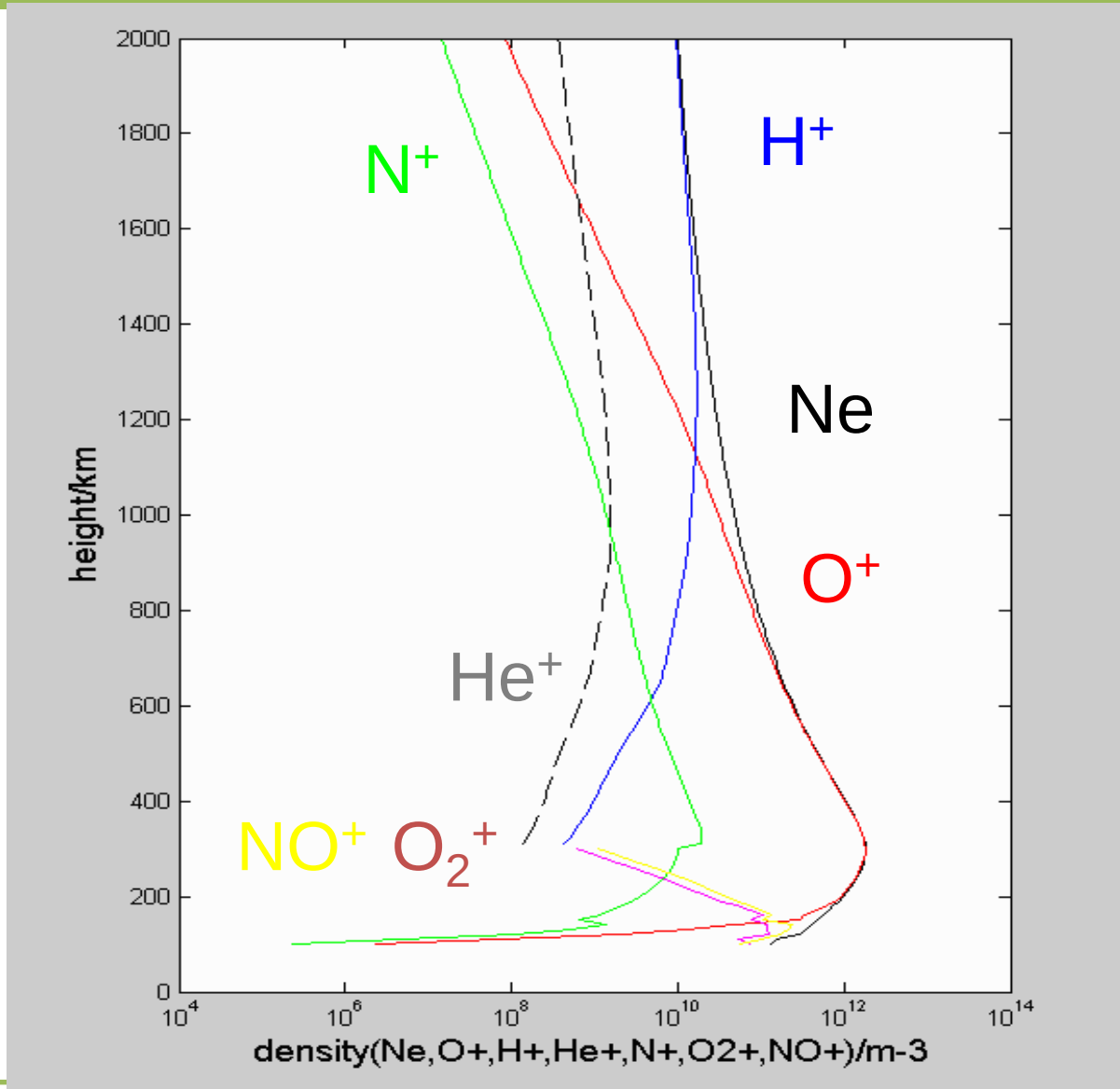

The upper transition height (Ht)

Altitude where the distribution of the dominant ions changes from the topside ionosphere (O^+) to the plasmasphere (H^+ and He^+)

Lower boundary of the plasmasphere O^+/H^+ or O^+/light ions (sum H^+ and He^+)

- Low solar activity – He^+ negligible – both heights almost identical
- High solar activity – both heights can differ by about several tens km or by 10% (Triskova et al., ASR, 1998)

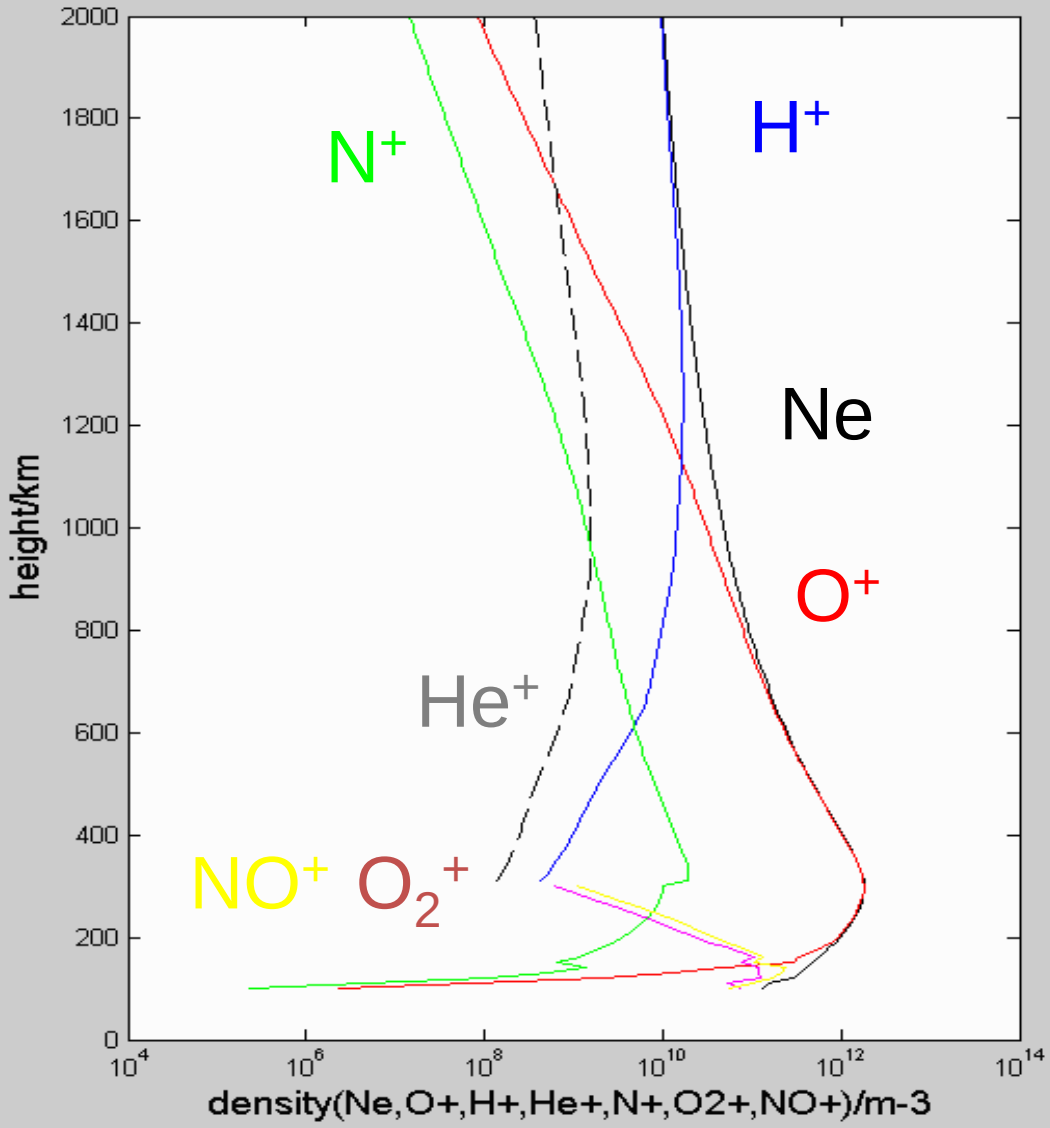

The upper transition height

IRI 2012

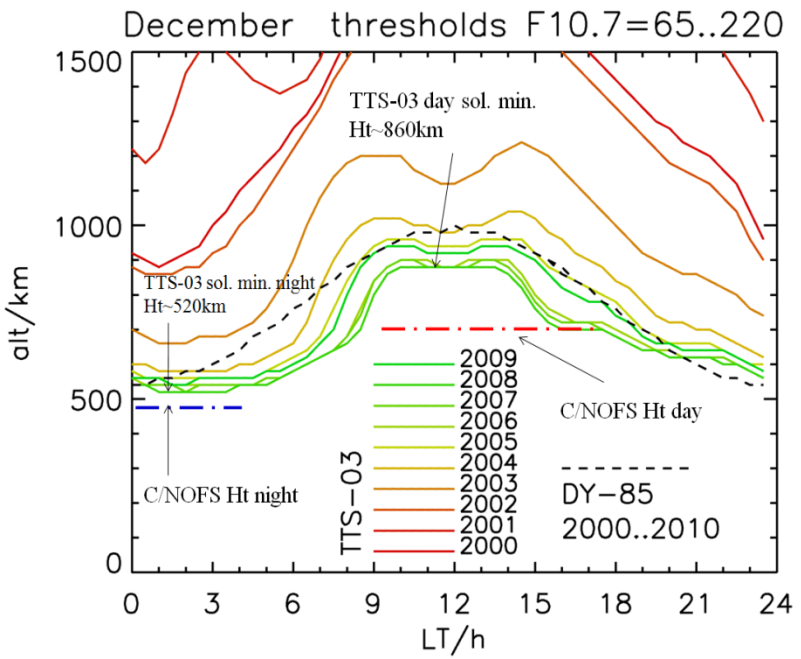

Ht strongly depends on solar activity!

DY-85 does not include this effect!

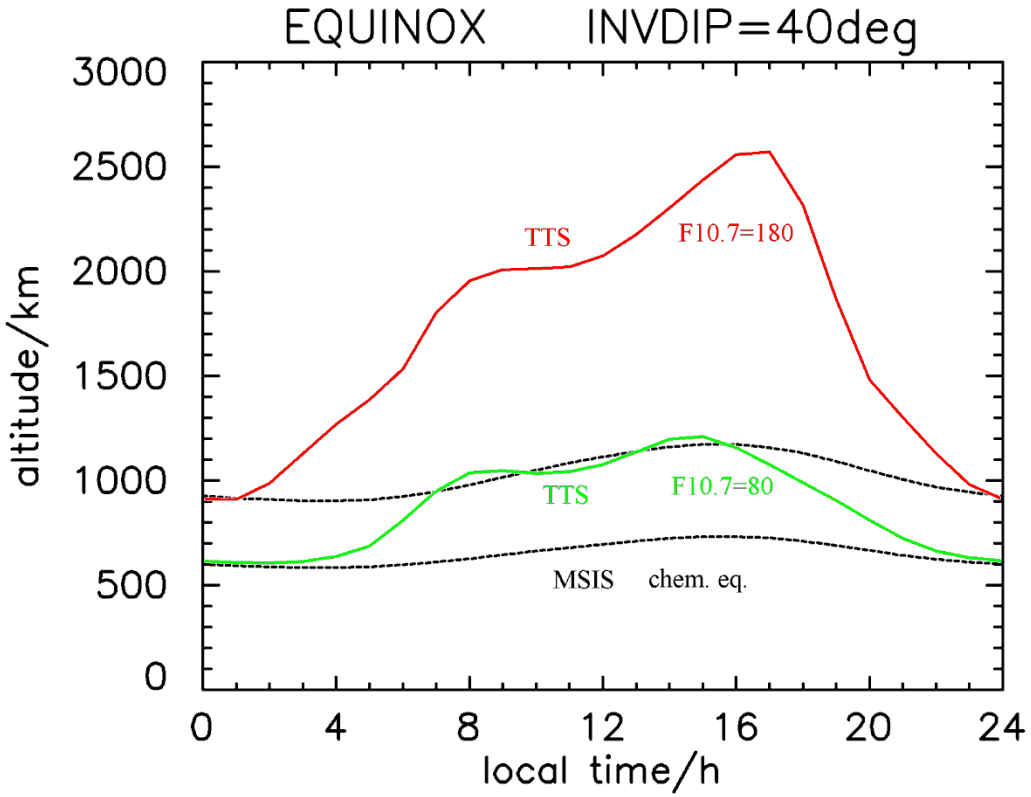

$$H^+ + O \underset{k2}{\overset{k1}{\rightleftharpoons}} O^+ + H \qquad k_1=2{,}5.10^{-11}\ T_n^{0,5} \qquad k_2=2{,}2.10^{-11}\ T_i^{0,5}$$

Chemical equilibrium: $[O]=9/8*[H]$ Very good approx. at night

Summary on ion composition

- Global models of ion composition included in IRI
  - Old DS-1995 & DY-1985
  - New RBV-2010 & TBT-15(default option)
- These models include most important dependencies (on latitude, altitude, local time, and solar activity)
- Only limited spatial resolution - up to 6th of spherical harmonics in topside
- More data is needed to better describe small scale features (anomalies, enhancements, troughs, longitudinal dependency etc.)
- We plan to better describe ion composition as a function of other parameters, especially as magnetic activity